Journal of Organometallic Chemistry 695 (2010) 2394–2400

Contents lists available at ScienceDirect

Journal of Organometallic Chemistry

journal homepage: www.elsevier.com/locate/jorganchem

The reactions of $Rh_2(CO)_4Cl_2$ with 1,5-cyclooctadiene and tetramethylallene. A combined in-situ vibrational spectroscopies, spectral reconstruction and DFT study

Feng Gao*, Chuanzhao Li, Effendi Widjaja, Chacko Jacob, Marc Garland*

Institute of Chemical & Engineering Sciences, 1 Pesek Road, Jurong Island, Singapore 627833, Singapore

ARTICLE INFO

Article history:
Received 19 April 2010
Received in revised form
14 July 2010
Accepted 16 July 2010
Available online 30 July 2010

Keywords:
Rhodium complexes
Tetramethylallene
In-situ spectroscopies
BTEM
DFT

ABSTRACT

Reactions of $Rh_2(CO)_4Cl_2$ with 1,5-cyclooctadiene (COD) and tetramethylallene (TMA) were performed separately in anhydrous hexane under argon atmosphere. Multiple perturbations of $Rh_2(CO)_4Cl_2$, COD and TMA were also performed during the reactions. These two reactions were monitored by in-situ FTIR (FIR and MIR) and/or Raman spectroscopies and the collected spectra were further analyzed with BTEM family of algorithms. DFT calculations were performed to identify the organometallic species present. The known diene complex $Rh_2(CO)_2Cl_2(\eta^4\text{-}C_8H_{12})$ and a new allene complex $Rh_2(CO)_3Cl_2(\eta^2\text{-}C_7H_{12})$ were formed as the two primary organo-rhodium products. Their pure component spectra were reconstructed in the three characteristic regions of 200–680, 800–1360, and 1500–2200 cm^{-1}. Their relative concentrations were also obtained by the least square fitting of the carbonyl region 1500-2200 cm^{-1}. The present contribution shows the usefulness of combining in-situ spectroscopic measurements, BTEM analysis and DFT spectral prediction in order to analyze organometallic reactions at high dilution and identify the reaction products.

1. Introduction

The coordination chemistry of $Rh_2(CO)_4Cl_2$ with simple ligands (L) has been the subject of a number of investigations. Ligands such as ethylene and phosphine can react with $Rh_2(CO)_4Cl_2$ to form substituted dinuclear complexes $Rh_2(CO)_{4-m}Cl_2L_m$ ($m = 1–4$) as well as mononuclear complexes $Rh(CO)_{3-n}ClL_n$, ($n = 1–3$) [1,2]. A cis-mononuclear complex $Rh(CO)_2Cl(py)$ was formed when pyridine(py) was used [3].

The dinuclear complex $Rh_2(CO)_2Cl_2(COD)$ is usually prepared from the reaction of (1) $Rh_2(CO)_4Cl_2$ with 1,5-cyclooctadiene directly [4]; or (2) $Rh_2Cl_2(COD)_2$ with $Rh_2(CO)_4Cl_2$ (1:1 molar ratio) in toluene [2]. Its crystal structure has been reported by Smith et al. in 2001 [5]. The structure consists of two dichloro-bridged rhodium atoms. The inter-conversion of $Rh_2(CO)_4Cl_2$, $Rh_2(CO)_2Cl_2(COD)$ and $Rh_2Cl_2(COD)_2$ can be described as shown in Scheme 1.

Reactions of sterically hindered tetramethylallene (TMA) with transition metal complexes have also been studied. In 1967, Pettit and Ben-Shoshan described the reaction of TMA with $Fe_2(CO)_9$ upon heating to form $Fe(CO)_4(\eta^2\text{-}C_7H_{12})$ as well as the intramolecular rearrangement to form a diene complex $Fe(CO)_3(\eta^4\text{-}C_7H_{12})$ [6]. Later on, the molecular structures of $(C_5H_7O_2)Rh(\eta^2\text{-}C_7H_{12})_2$ and $[Cl_2Pt\text{-}(C_7H_{12})]_2{\cdot}2CCl_4$ were determined by single-crystal XRD [7,8]. In most cases, the tetramethylallene ligand coordinates to the metal center in a manner similar to η^2-bonded mono-olefin [6–10]. With respect to the coordination chemistry of TMA with the precursor $Rh_2(CO)_4Cl_2$, no detailed studies have been reported so far.

In-situ vibrational spectroscopies have been successfully used in combination with band-target entropy minimization (BTEM) spectral analysis and density functional (DFT) calculations to better understand the detailed chemistry of many organometallic and homogeneous catalyzed reactions, particular those involving rhodium carbonyl complexes [11,12]. BTEM [13,14] is essentially a self modeling curve resolution (SMCR) approach to obtain the pure component spectra of species without any a priori information. The algorithm searches for the simplest underlying patterns in a data set regardless of its origin. The simplest patterns are usually those which possess the lowest signal entropy.

$$Rh_2(CO)_4Cl_2 \underset{CO}{\overset{COD}{\rightleftharpoons}} Rh_2(CO)_2Cl_2(COD) \underset{CO}{\overset{COD}{\rightleftharpoons}} Rh_2Cl_2(COD)_2$$

Scheme 1. The inter-conversion of $Rh_2(CO)_4Cl_2$, $Rh_2(CO)_2Cl_2(COD)$ and $Rh_2Cl_2(COD)_2$.

* Corresponding authors.
E-mail addresses: gao_feng@ices.a-star.edu.sg (F. Gao), marc_garland@ices.a-star.edu.sg (M. Garland).

0022-328X/$ – see front matter © 2010 Elsevier B.V. All rights reserved.
doi:10.1016/j.jorganchem.2010.07.018

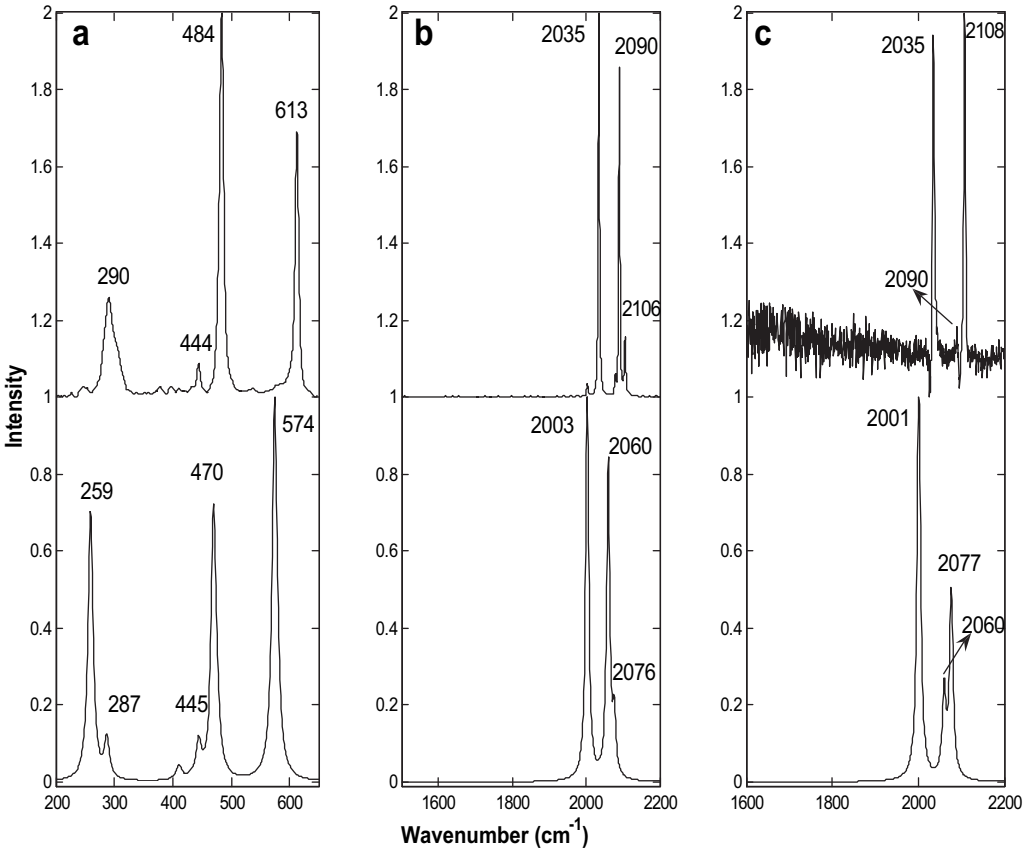

Fig. 1. DFT predicted spectra of the precursor $Rh_2(CO)_4Cl_2$ and its corresponding references in the regions of 200–650 (FIR, Rh–Cl, Rh–C vibrations), 1500–2200 (MIR), and 1600–2200 (Raman) cm^{-1}. Top: References (a,c: BTEM estimates; b, Experimental reference); Bottom: DFT predicted spectra.

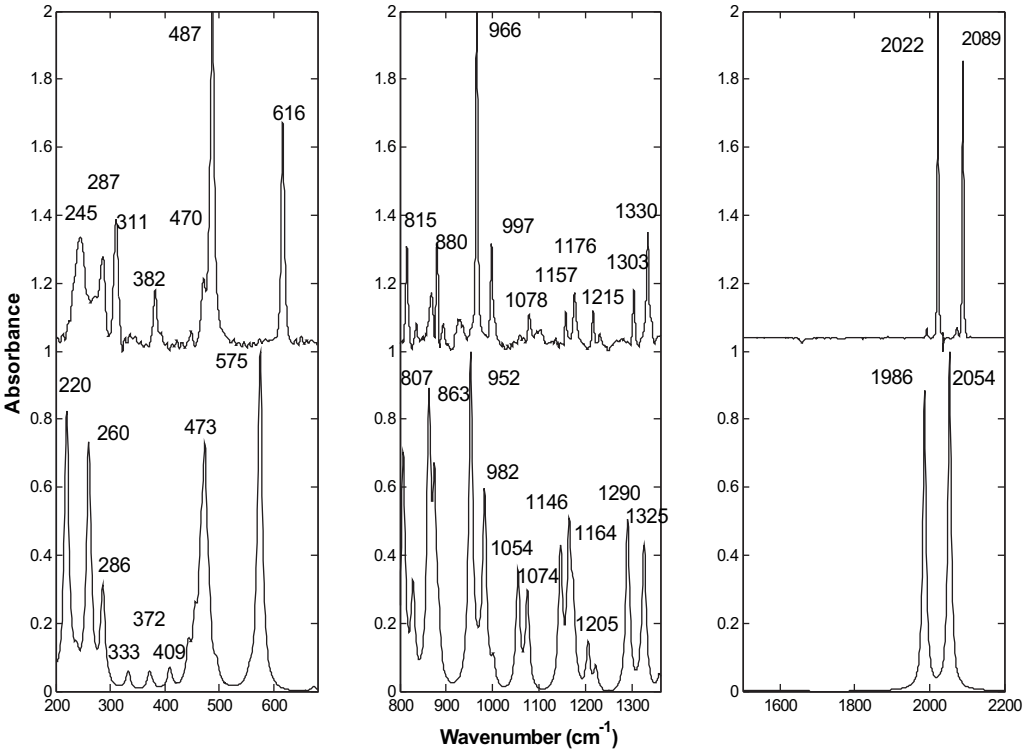

Fig. 2. BTEM estimates and DFT predicted spectra of the complex $Rh_2(CO)_2Cl_2(\eta^4\text{-}C_8H_{12})$ in the IR regions of 200–680, 800–1360, and 1500–2200 cm^{-1}. Top: BTEM estimates; Bottom: DFT predicted spectra.

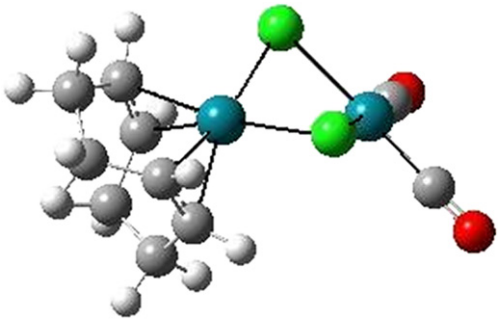

Fig. 3. The optimized geometry of $Rh_2(CO)_2Cl_2(\eta^4\text{-}C_8H_{12})$.

In the present contribution, both FIR and low wavenumber MIR measurements were used, in addition to MIR and Raman in the carbonyl range, in order to better understand the coordination chemistry of COD and TMA with $Rh_2(CO)_4Cl_2$. The BTEM analysis of the data provided spectral estimates of five carbonyl complexes, namely, the precursor $Rh_2(CO)_4Cl_2$, one known complex $Rh_2(CO)_2Cl_2(\eta^4\text{-}C_8H_{14})$, one new complex $Rh_2(CO)_3Cl_2(\eta^2\text{-}C_7H_{12})$ and 2 minor and presently un-assigned species. DFT calculations allowed the assignment for the new complex $Rh_2(CO)_3Cl_2(\eta^2\text{-}C_7H_{12})$ without the separation or purification of the species from the solution.

2. Experimental

2.1. General information

All solution preparations and transfers were performed with Schlenk techniques [15] under argon (99.999%, Soxal, Singapore). The solvent hexane (99.6%+, Fluka) was refluxed for ca. 5 h over sodium-potassium alloy under argon. Rhodium carbonyl chloride (99%, Strem), 1,5-cyclooctadiene (99%, Sigma–Aldrich) and TMA (97%, Sigma–Aldrich) were used as received.

2.2. Equipment setup and in-situ spectroscopic measurements

A Bruker FTIR spectrometer (Vertex 70) with deuterated triglycine sulfate (DTGS) detector was used. Spectral resolution was 2 cm^{-1} for the MIR region of 400–5000 cm^{-1}. Spectral resolution was 4 cm^{-1} for the FIR region of 30–700 cm^{-1} and a cell with diamond windows was used for these measurements. Purified compressed air was used to purge the FTIR spectrometer system. In-situ Raman spectra in the region of 100–2400 cm^{-1} were recorded with a dispersive-type Raman microscope (InVia Reflex

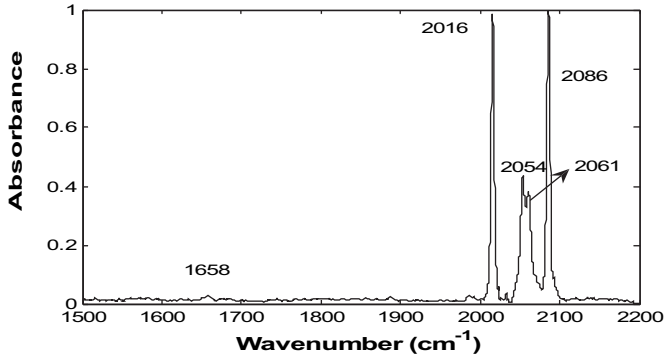

Fig. 4. BTEM estimate of the minor species (species 2) in the region of 1500–2200 cm^{-1}.

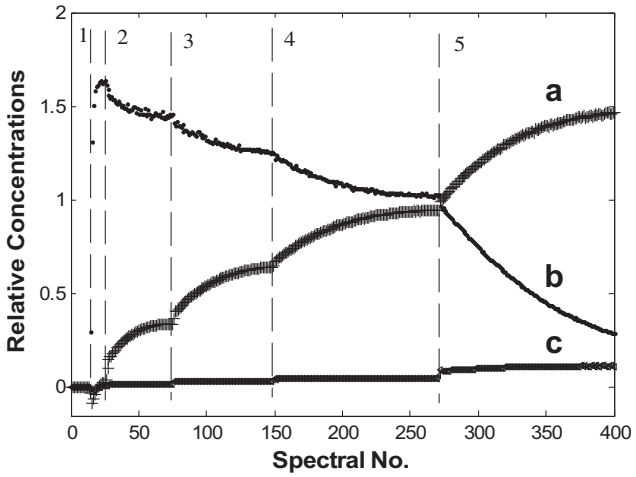

Fig. 5. Relative concentration profiles for the organometallic species present in the system. (a) $Rh_2(CO)_2Cl_2(\eta^4\text{-}C_8H_{12})$; (b) $Rh_2(CO)_4Cl_2$; (c) the minor species 2. Five perturbations performed: region 1 involved the addition of 152.3 mg $Rh_2(CO)_4Cl_2$; regions 2–4 involved the injection of 250 μL COD stock solution (20 μL COD dissolved in 1 ml hexane) each; and region 5 involved the injection of 300 μL COD.

Renishaw, UK). The laser source used was a 785 nm near-infrared diode laser with 100% power (ca. 100 mW on the sample) and an exposure time of ca. 30 s. The in-situ spectroscopic measurements were performed at room temperature (ca. 24 °C).

The general experimental system has been reported elsewhere [11,12]. The reaction of COD/TMA with rhodium carbonyl chloride was performed under argon with multiple perturbations. Reaction was initiated by the injection of a certain amount of COD/TMA solution through the rubber septum. At pre-determined times, various perturbations of COD/TMA solution and rhodium carbonyl chloride solution were performed. It is well documented that multiple perturbation experiments greatly improve the quality of spectral reconstructions via BTEM.

2.3. Spectral reconstruction via BTEM family of algorithms

The original band-target entropy minimization algorithm has been extensively used to reconstruct the pure component spectra from various spectral data. Recently, multi-reconstruction entropy minimization (MREM) [16] was developed in order to first survey the underlying spectral patterns. Subsequently, based on these initial local spectral estimates via MREM, the pure component spectral estimates can be further refined using either BTEM or tBTEM [17]. In the present study, a combination of MREM and BTEM/tBTEM were used.

2.4. Density functional calculations

Gaussian 03 [18] was used for all the calculations in this study. The geometric optimizations were performed using PBEPBE density function with DGDZVP basis set plus solvent effect of heptane and the FIR/MIR/Raman vibrational frequencies were calculated afterwards. The appropriateness of this density function and basis set as a predictive tool for the terminal and bridged C=O vibrations of rhodium carbonyl chloride complexes was verified with the precursor $Rh_2(CO)_4Cl_2$. The FIR (200–650 cm^{-1}) and Raman BTEM estimates (1600–2200 cm^{-1}), MIR experimental reference (1500–2200 cm^{-1}) as well as the DFT predicted spectral estimates for the precursor are plotted in Fig. 1. These DFT predicted FTIR and Raman spectra were normalized after they were exported through GaussView 3.0.9

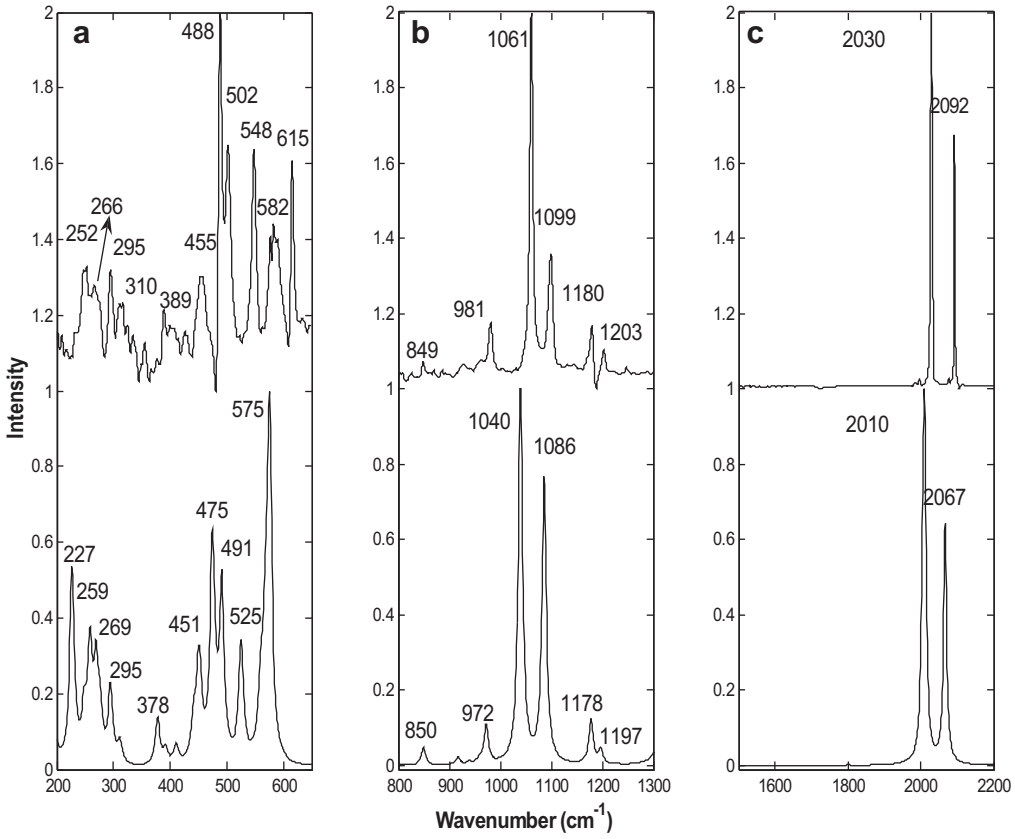

Fig. 6. BTEM estimates and DFT predicted spectra of the complex $Rh_2(CO)_3Cl_2(\eta^2\text{-}C_7H_{12})$ in the regions of 200–650, 800–1300, and 1500–2200 cm^{-1}. Top: BTEM estimates; Bottom: DFT predicted spectra.

and cut into the three corresponding regions. The optimized geometry and the DFT predicted vibrational wavenumbers were consistent with the available experimental references [19,20]. The predicted four equivalent bond lengths of Rh–Cl in $Rh_2(CO)_4Cl_2$ are 2.45 Å and this can be compared to the experimental value of 2.384 Å from the crystal structure. The distance between the two Rh atoms is 3.18 Å for the DFT predicted structure while the distance is 3.138Å for the crystal structure. The Rh_2Cl_2 core is obviously non-planar, the predicted dihedral angle about the Cl···Cl hinge is ca. 121° while it is ca. 128.6° in the crystal.

In general, the DFT calculations tend to underestimate the vibrational wavenumbers by ca. 0–2% for the C–H, C–C and C=O, ca. 1–7% for the Rh–C and ca. 10% for Rh–Cl. Therefore, it appears that the present density functional method can be used as a predictive tool in this study.

The assignment of the species observed in this study was made based on consistency between the DFT predicted spectra and the BTEM spectral estimates as well as the consideration of the potential solution chemistry.

3. Results and discussion

3.1. Coordination chemistry of $Rh_2(CO)_4Cl_2$ with 1,5-cyclooctadiene (COD)

The experimental spectra from the reaction of $Rh_2(CO)_4Cl_2$ with 1,5-cyclooctadiene (COD) were cut into three regions, namely

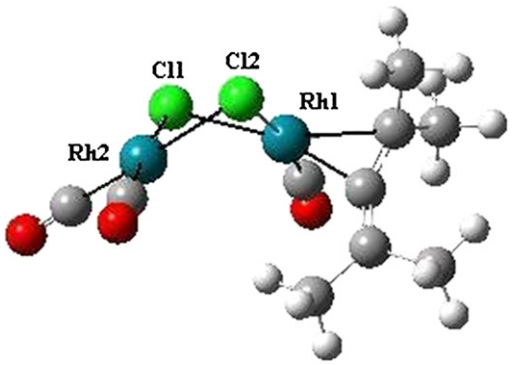

Fig. 7. The optimized geometry of $Rh_2(CO)_3Cl_2(\eta^2\text{-}C_7H_{12})$.

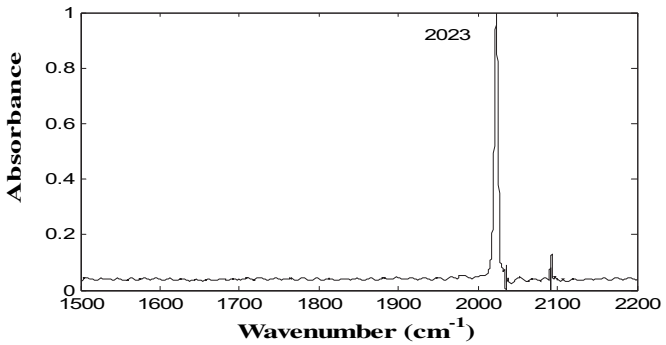

Fig. 8. BTEM estimate of the minor species 3 in the region of 1500–2200 cm^{-1}.

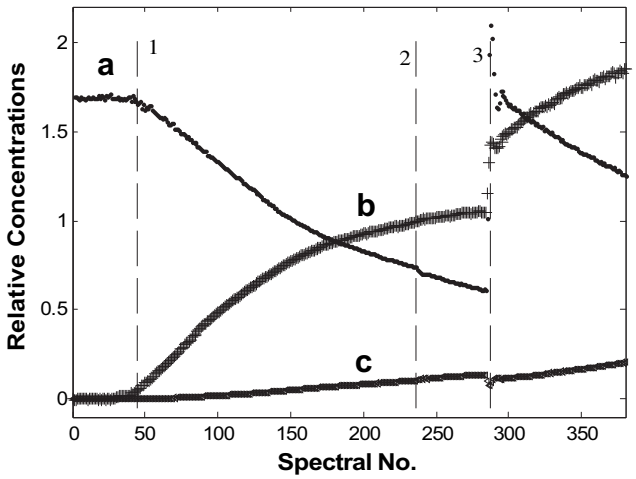

Fig. 9. Relative concentration profiles for the organometallic species present in the system. (a) $Rh_2(CO)_4Cl_2$; (b) $Rh_2(CO)_3Cl(\eta^2\text{-}C_7H_{12})$; (c) the minor species 3. Three perturbations performed: region 1 involved the continuous feeding of TMA stock solution (25 μL/min, 2 h, ca. 171 μL TMA was injected in total); region 2 involved the injection of 100 μL TMA; and region 3 involved the addition of 72.3 mg of $Rh_2(CO)_4Cl_2$.

200–680, 800–1360, and 1500–2200 cm^{-1}, and further processed with the BTEM family of algorithms. The FIR/MIR BTEM estimates of $Rh_2(CO)_2Cl_2(\eta^4\text{-}C_8H_{14})$ in three regions as well as their corresponding DFT predicted spectra are shown in Fig. 2. It can be seen from this figure that the DFT predicted and the BTEM estimated wavenumbers show a systematic deviation of 0–2% in the MIR region and ca. 1–10% in the FIR region. Therefore the DFT predicted spectra are fairly consistent with the BTEM estimates in the three regions.

The optimized geometry of $Rh_2(CO)_2Cl_2(\eta^4\text{-}C_8H_{14})$ is plotted in Fig. 3. The structure consists of two square-planar Rh atoms bridged by two Cl atoms. The distance between two Rh atoms is 3.11 Å for the DFT predicted structure while the distance for the crystal structure is 3.284 Å. The Rh_2Cl_2 core is obviously non-planar, the dihedral angle about the Cl···Cl hinge is ca. 121° while the dihedral angle for the crystal structure is ca. 139.6°. Accordingly, the bond lengths and angles predicted by DFT are similar, but not exactly equal to the experimentally determined solid state structure.

In addition, one other pure component spectrum (species 2, Fig. 4) with maxima at 2016, 2054, 2061, 2086 cm^{-1} was obtained from BTEM analysis. The signal contribution of this pure component spectrum is low and accordingly, the BTEM estimate corresponds to a minor species in the system. The band pattern shown in Fig. 4 suggests that species may be a dinuclear with low symmetry and 4 carbonyl groups.

The BTEM estimates of $Rh_2(CO)_2Cl_2(\eta^4\text{-}C_8H_{12})$ and species 2 as well as the experimental references of cell plus hexane and $Rh_2(CO)_4Cl_2$ were used in the least squares fit of the reactions spectra obtained in the region 1500–2200 cm^{-1}. The calculated relative concentrations are plotted in Fig. 5. Almost 100% signal recovery was obtained. It can be seen from this figure that at the end of the reaction there was ca. 18% of $Rh_2(CO)_4Cl_2$ left in the reaction system. Therefore $Rh_2(CO)_2Cl_2(\eta^4\text{-}C_8H_{12})$ was the predominant species during the whole reaction time.

3.2. Coordination chemistry of $Rh_2(CO)_4Cl_2$ with tetramethylallene (TMA)

The experimental spectra from the reaction of $Rh_2(CO)_4Cl_2$ with TMA were cut into three regions, namely 200–650, 800–1300, and 1500–2200 cm^{-1}, then further processed with the BTEM family of algorithms. The FIR/MIR BTEM estimates of the new complex as well as the DFT predicted spectra of $Rh_2(CO)_3Cl_2(\eta^2\text{-}C_7H_{12})$ are shown in Fig. 6. It can be seen from this figure that the DFT predicted wavenumbers and the BTEM estimated wavenumbers show a systematic deviation of 0–2% in the MIR region and ca. 1–10% in the FIR region. Therefore, there is considerable consistency between the BTEM spectral estimates and the DFT predicted spectra in the MIR, as well as reasonable consistency in the FIR.

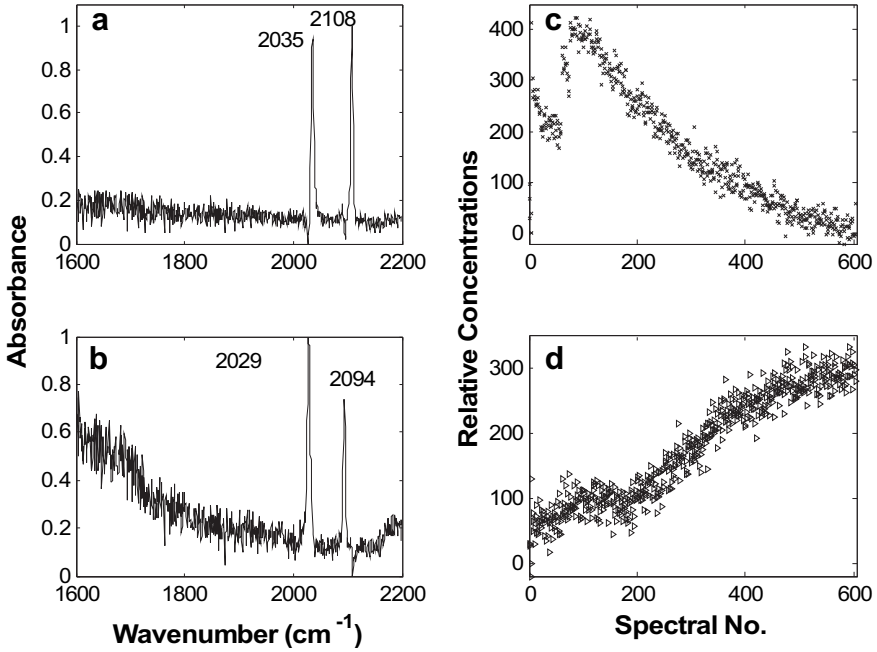

Fig. 10. Raman BTEM estimates of $Rh_2(CO)_4Cl_2$ and $Rh_2(CO)_3Cl_2(\eta^2\text{-}C_7H_{12})$ and their corresponding relative concentrations in the region of 1600–2200 cm^{-1} (a,c) $Rh_2(CO)_4Cl_2$; (b,d) $Rh_2(CO)_3Cl_2(\eta^2\text{-}C_7H_{12})$.

Similar differences between the BTEM estimated spectra and the DFT predicted spectra of $Rh_2(CO)_2Cl_2(\eta^4\text{-}C_8H_{12})$ were observed.

The optimized geometry of $Rh_2(CO)_3Cl_2(\eta^2\text{-}C_7H_{12})$ is plotted in Fig. 7. The structure consists of two square-planar Rh atoms bridged by two Cl atoms. The predicted bond lengths and angles of rhodium 2 are similar to those predicted in the $Rh_2(CO)_4Cl_2$. The bond length of Rh_2-Cl_1 is 2.44 Å and the bond length of Rh_2-Cl_2 is 2.44 Å. The Rh_2Cl_2 core is obviously non-planar, the dihedral angle about the Cl···Cl hinge is ca. 121° which is same as that of $Rh_2(CO)_4Cl_2$.

In addition, one other pure component spectrum (species 3, Fig. 8) with maxima at 2023 cm^{-1} was obtained from the BTEM analysis. The signal contribution of this pure component spectrum is low and accordingly, the BTEM estimate corresponds to a minor species in the system.

A combination of BTEM estimates of $Rh_2(CO)_3Cl_2(\eta^2\text{-}C_7H_{12})$ and species 3 and experimental reference of cell plus hexane and $Rh_2(CO)_4Cl_2$ were used in the least squares fit of the reaction spectra obtained in the carbonyl region. The calculated relative concentrations are plotted in Fig. 9. During the 3rd perturbation, ca. 72.3 mg of $Rh_2(CO)_4Cl_2$ was added and a rapid increase of the concentrations of $Rh_2(CO)_4Cl_2$ and $Rh_2(CO)_3Cl_2(\eta^2\text{-}C_7H_{12})$ was observed afterwards. Almost 100% signal recovery was obtained. This figure confirms that $Rh_2(CO)_4Cl_2$ and $Rh_2(CO)_3Cl_2(\eta^2\text{-}C_7H_{12})$ were the major species present during reaction.

In addition, in-situ Raman spectroscopic measurement was also performed for this reaction. The obtained spectra were visually inspected and the region of 1600–2200 cm^{-1} was selected for the further BTEM analysis. The Raman BTEM estimates of $Rh_2(CO)_4Cl_2$ and $Rh_2(CO)_3Cl_2(\eta^2\text{-}C_7H_{12})$ in the region of 1600–2200 cm^{-1} are plotted in Fig. 10(a & b). Their corresponding relative concentrations are also plotted in Fig. 10(c & d). It can be seen from this figure that the concentrations of $Rh_2(CO)_3Cl_2(\eta^2\text{-}C_7H_{12})$ increase gradually with time.

4. Discussion

In-situ FTIR and Raman measurements were combined with signal processing and DFT calculations in order to better understand the reactions of $Rh_2(CO)_4Cl_2$ with COD and TMA. The major species formed were a known diene complex $Rh_2(CO)_2Cl_2(\eta^4\text{-}C_8H_{12})$ and a new allene complex $Rh_2(CO)_3Cl_2(\eta^2\text{-}C_7H_{12})$. The assignments were made based on consistency between the DFT predicted spectra and the BTEM estimates, as well as consideration of the potential coordination chemistry.

One minor species, species 2, was reconstructed during the reaction of 1,5-COD with $Rh_2(CO)_4Cl_2$. It has four maxima at ca. 2016, 2054, 2061, 2086 cm^{-1} in the carbonyl region. The other minor species with a maximum at ca. 2023 cm^{-1} was reconstructed during the reaction of TMA with $Rh_2(CO)_4Cl_2$. The two BTEM estimates are not consistent with the impurities $Fe(CO)_5$, $Ni(CO)_4$, and $Mo(CO)_6$ which have sometimes been detected in our other in-situ spectroscopic studies [21]. Due to the low concentrations of these two minor species, their FIR and low wavenumber MIR spectra could not be obtained and therefore their identification is not presently possible. These two species might be associated with: (1) species arising from reactions with impurities in the reaction system or (2) side reactions not considered in this study.

Differences were observed between the DFT predicted frequencies and the BTEM estimates for all three major organometallic species. Smaller deviations of 0–2% were observed in the carbonyl and low wavenumber MIR region and larger deviations of 1–10% were observed for the Rh–Cl and Rh–C vibrations. Deviations were also observed between the DFT predicted bond lengths and the experimental value for Rh–Cl and Rh–Rh. This difference may be due to the difficulties in accurately modeling the electron density associated with the Rh–Cl, Rh–Rh and Rh–C bonds. Indeed, even the accurate prediction of the vibrational frequency and bond length associated with C–Cl in organic molecules can pose difficulties.

In-situ NMR and vibrational studies are the clearly preferred approaches to identify intermediates in organometallic chemistry and homogeneous catalysis [22]. The primary advantage of NMR is that very detailed structural information can be readily obtained. The primary advantage of vibrational spectroscopies is that parts-per-million detectability is entirely realistic. But less information about the detailed structure is usually available.

Some recent signal processing advances including the development of BTEM family of algorithms enables the spectral reconstruction of the species at parts-per-million concentration level or less [14,15]. Very good signal-to-noise spectral reconstructions can be obtained for most of species present, i.e., those that are responsible for more than ca. 0.1% of the total measured spectroscopic signals. At this level of signal intensity, the pure component spectra can be reliably mapped back onto the original data in order to obtain relative and even absolute concentrations. This is the case occurred in this study.

5. Conclusion

A combination of in-situ FTIR/Raman spectroscopic measurements, BTEM deconvolution and DFT calculations were successfully used to study the reactions of $Rh_2(CO)_4Cl_2$ with COD and TMA. One known diene complex $Rh_2(CO)_2Cl_2(\eta^4\text{-}C_8H_{12})$ and one new allene complex $Rh_2(CO)_3Cl_2(\eta^2\text{-}C_7H_{12})$ were formed as the primary species respectively. The pure component spectra of these two species in the FIR (200–680 cm^{-1}) and MIR (800–1360 and 1500–2200 cm^{-1}) regions were successfully obtained with the application of BTEM family of algorithms and without the separation or purification from the solution. This study demonstrate that with the combination of in-situ spectroscopic study, BTEM algorithm and DFT calculations, some of the diverse and complex coordination chemistries that can occur between $Rh_2(CO)_4Cl_2$ and diene/allene can be addressed.

Acknowledgement

This work was supported by the Science and Engineering Research Council of A*STAR (Agency for Science, Technology and Research), Singapore.

References

[1] J. Gallay, D. de Montauzon, R. Poilblanc, J. Organometal. Chem. 38 (1972) 179–197.
[2] A. Maisonnat, P. Kalck, R. Poilblanc, Inorg. Chem. 13 (1974) 661–667.
[3] B.T. Heaton, C. Jacob, J.T. Sampanthar, J. Chem. Soc. Dalton Trans. (1998) 1403–1410.
[4] J. Chatt, L.M. Venanzi, J. Chem. Soc. (1957) 4735–4741.
[5] M. Abou Rida, J. Saikaili, A.K. Smith, A. Thozet, Acta Cryst. C57 (4) (2001) 352–353.
[6] R. Ben-Shoshan, R. Pettit, J. Am. Chem. Soc. 89 (1967) 2231–2232.
[7] T.G. Hewitt, K. Anzenhofer, J.J. De Boer, Chem. Comm. 6 (1969) 312–313.
[8] T.G. Hewitt, J.J. De Boer, J. Chem. Soc. A 6 (1971) 817–822.
[9] P. Racanellani, G. Pantini, A. Immirzi, G. Allegra, L. Porri, J. Chem. Soc. D: Chem. Comm. (1969) 361–362.
[10] K. Vrieze, H.C. Volger, A.P. Praat, J. Organometal. Chem. 21 (2) (1970) 467–475.
[11] A.D. Allian, M. Tjahjono, M. Garland, Organometallics 25 (9) (2006) 2182–2188.
[12] A.D. Allian, E. Widjaja, M. Garland, J. Chem. Soc. Dalton Trans. (2006) 4211–4217.
[13] W. Chew, E. Widjaja, M. Garland, Organometallics 21 (9) (2002) 1982–1990.
[14] E. Widjaja, C.Z. Li, M. Garland, Organometallics 21 (2002) 1991–1997.
[15] D.F. Shriver, M.A. Drezdzon, The Manipulation of Air-Sensitive Compounds. Wiley, 1986.
[16] H.J. Zhang, W. Chew, M. Garland, Appl. Spectrosc. 61 (2007) 1366–1372.
[17] F. Gao, H.J. Zhang, L.F. Guo, M. Garland, Chemom. Intell. Lab. Syst. 95 (2009) 94–100.

[18] M.J. Frisch, G.W. Trucks, H.B. Schlegel, G.E. Scuseria, M.A. Robb, J.R. Cheeseman, J.A. Montgomery Jr., T. Vreven, K.N. Kudin, J.C. Burant, J.M. Millam, S.S. Iyengar, J. Tomasi, V. Barone, B. Mennucci, M. Cossi, G. Scalmani, N. Rega, G.A. Petersson, H. Nakatsuji, M. Hada, M. Ehara, K. Toyota, R. Fukuda, J. Hasegawa, M. Ishida, T. Nakajima, Y. Honda, O. Kitao, H. Nakai, M. Klene, X. Li, J.E. Knox, H.P. Hratchian, J.B. Cross, V. Bakken, C. Adamo, J. Jaramillo, R. Gomperts, R.E. Stratmann, O. Yazyev, A.J. Austin, R. Cammi, C. Pomelli, J. Ochterski, P.Y. Ayala, K. Morokuma, G.A. Voth, P. Salvador, J.J. Dannenberg, V.G. Zakrzewski, S. Dapprich, A.D. Daniels, M.C. Strain, O. Farkas, D.K. Malick, A.D. Rabuck, K. Raghavachari, J.B. Foresman, J.V. Ortiz, Q. Cui, A.G. Baboul, S. Clifford, J. Cioslowski, B.B. Stefanov, G. Liu, A. Liashenko, P. Piskorz, I. Komaromi, R.L. Martin, D.J. Fox, T. Keith, M.A. Al-Laham, C.Y. Peng, A. Nanayakkara, M. Challacombe, P.M.W. Gill, B.G. Johnson, W. Chen, M.W. Wong, C. Gonzalez, J.A. Pople, GAUSSIAN03 (RevisionC.02). Gaussian, Inc., Wallingford, CT, 2004.
[19] L.F. Dahl, C. Martell, D.L. Wampler, J. Am. Chem. Soc. 83 (1961) 1762–1763.
[20] L. Walz, P. Scheer, Acta Cryst. C47 (1991) 640–641.
[21] A.D. Allian, M. Garland, Dalton Trans. (2005) 1957–1965.
[22] B. Heaton (Ed.), Mechanisms in Homogeneous Catalysis: A Spectroscopic Approach, Wiley-VCH, 2005.